CONF-961102--4

GA-A22521

INVESTIGATION OF PHYSICAL PROCESSES LIMITING PLASMA DENSITY IN H-MODE ON DIII-D

by

R. MAINGI, M.A. MAHDAVI, T.C. JERNIGAN, R.J. LA HAYE, L.R. BAYLOR, D.G.WHYTE, M.R. WADE, T.W. PETRIE, J.W. CUTHBERTSON, A.W. LEONARD, M. MURAKAMI, R.T. SNIDER, R.D. STAMBAUGH, J.G. WATKINS, W.P. WEST, and R.D. WOOD

MASTER

DECEMBER 1996

GENERAL ATOMICS

GA–A22521

INVESTIGATION OF PHYSICAL PROCESSES LIMITING PLASMA DENSITY IN H–MODE ON DIII–D

by

R. MAINGI,[1] M.A. MAHDAVI, T.C. JERNIGAN,[2] R.J. LA HAYE, L.R. BAYLOR,[2] D.G.WHYTE,[3] M.R. WADE,[2] T.W. PETRIE, J.W. CUTHBERTSON,[4] A.W. LEONARD, M. MURAKAMI,[2] R.T. SNIDER, R.D. STAMBAUGH, J.G. WATKINS,[5] W.P. WEST, and R.D. WOOD[6]

This is a preprint of an invited paper presented at the APS Division of Plasma Physics Meeting, November 11–15, 1996, Denver, Colorado, and to be printed in a Special Issue of *Physics of Plasmas.*

Work supported by U.S. Department of Energy Contracts DE-AC03-89ER51114, DE-AC05-96OR22464, DE-AC04-94AL85000 and W-7405-ENG-48, and Grant DE-FG03-86ER53266

[1]ORAU Postdoctoral Fellow
[2]Oak Ridge National Laboratory
[3]Centre Canadien de Fusion Magnétique
[4]University of California, Los Angeles
[5]Sandia National Laboratories
[6]Lawrence Livermore National Laboratory

GENERAL ATOMICS PROJECT 3466
DECEMBER 1996

Investigation of physical processes limiting plasma density in high confinement mode discharges on DIII–D

R. Maingi,[a] M.A. Mahdavi, T.C. Jernigan,[b] R.J. La Haye, A.W. Hyatt, L.R. Baylor,[b] D.G. Whyte,[c] M.R. Wade,[b] T.W. Petrie, J.W. Cuthbertson,[d] A.W. Leonard, M. Murakami,[b] R.T. Snider, R.D. Stambaugh, J.G. Watkins,[e] W.P. West, and R.D. Wood[f]

General Atomics, P.O. Box 85608, San Diego, California 92186-5608

A series of experiments was conducted on the DIII–D tokamak [J.L. Luxon and L.G. Davis, Fusion Technol. **8**, 441 (1985)] to investigate the physical processes which limit density in high confinement mode (H–mode) discharges. The typical H–mode to low confinement mode (L–mode) transition limit at high density near the empirical Greenwald density limit [M. Greenwald, J.L. Terry, S.M. Wolfe, S. Ejima, M.G. Bell, S.M. Kaye, and G.H. Neilson, Nucl. Fusion **28**, 2199 (1988)] was avoided by divertor pumping, which reduced divertor neutral pressure and prevented formation of a high density, intense radiation zone (MARFE) near the X–point. It was determined that the density decay time after pellet injection was independent of density relative to the Greenwald limit and increased non-linearly with the plasma current. Magnetohydrodynamic (MHD) activity in pellet-fueled plasmas was observed at all power levels, and often caused unacceptable confinement degradation, except when the neutral beam injected (NBI) power was ≤ 3 MW. Formation of MARFEs on closed field lines was avoided with low safety factor (q) operation but was observed at high q, qualitatively consistent with theory. By using pellet fueling and optimizing discharge parameters to avoid each of these limits, an operational space was accessed in which density $\sim 1.5\times$ Greenwald limit was achieved for 600 ms, and good H–mode confinement was maintained for 300 ms of the density flat-top. More significantly, the density was successfully increased to the limit where a central radiative collapse was observed, the most fundamental density limit in tokamaks.

---

[a]Oak Ridge Associated Universities Fellow at General Atomics.
[b]Oak Ridge National Laboratory, Oak Ridge, Tennessee 37831.
[c]Centre Canadien de Fusion Magnétique, Québec, Canada.
[d]University of California, Los Angeles, California 90024.
[e]Sandia National Laboratories, Albuquerque, New Mexico 87185-5800.
[f]Lawrence Livermore National Laboratory, Livermore, California 94551.

CONTENTS

Figures

I. INTRODUCTION

Scaling of experimental data from many tokamaks with gas fueling has indicated the presence of a maximum electron density above which the frequency of disruptive terminations increases rapidly. Disruptive termination at the density limit is frequently correlated with growth of low m,n magnetohydrodynamic (MHD) modes. By examining data both from ohmically-heated and neutral beam-heated tokamak discharges, Greenwald *et al.* concluded[1] that this disruptive limit was given by $\bar{n}_e^{max} \cong \kappa \bar{J}$ where κ is the elongation and $\bar{J}$ is the average plasma current density. For elliptical plasmas, the relation reduces to $\bar{n}_e^{max} \cong I_p/\pi a^2$, where $\bar{n}_e^{max}$ is in 10^{20} m^{-3}, I_p is the plasma current in MA, and a is the minor radius in meters. Several theories[2–5] have reproduced the I_p/a^2 scaling for ohmically-heated plasmas and these theories suggested that the scaling originates from an edge plasma power balance limit. The constraint exists because both the heating level and MHD stability are determined by the current density profile. However, Greenwald's dataset included auxiliary-heated, low-confinement mode (L–mode) plasmas. Therein lies the conundrum — if the density limit is an edge power balance limit, then why do not auxiliary-heated discharges always exhibit a higher density limit? Considering either the central or edge/scrape-off layer (SOL) power balance (*e.g.*, in Ref. 6), the maximum density [$\bar{n}_e$ (DL)] is expected to increase with the heating power (P_{heat}), *i.e.*, $\bar{n}_e(\mathrm{DL}) \propto P_{heat}^{\alpha}$, where $0.5 \le \alpha \le 0.7$. Data from the ASDEX tokamak with the "DV I" divertor geometry indicated a density limit power dependence with $\alpha \sim 0.5$, but modification of the divertor leading to a more closed geometry ("DV II") weakened this dependence to $\alpha \sim 0.25$.[7,8] A density limit power dependence with $\alpha \sim 0.5$ has been reported for low confinement (L–mode) limiter discharges[9] from the Joint European Torus (JET),[10] but this dependence was reduced in diverted discharges with the Mark I configuration.[11] Similarly, JT-60[12] reported a density limit power dependence with $\alpha \sim 0.5$ in L–mode limiter discharges,[13] but a systematic study to determine the density limit in high confinement (H–mode) diverted discharges on JT-60U has not been done.[14] [Hence a strong power dependence has not been established in all configurations and confinement modes. Based on discharges from the Alcator-C tokamak,[15] Greenwald concluded that the limit was caused by an increase in particle transport at high density, *i.e.,* not related to an edge power balance directly. With sufficient central fueling from pellets, the density was transiently increased above $\bar{n}_e^{max}$ in Alcator-C discharges, and a rapid decrease in particle confinement time was observed. Experiments[13,16,17] from JT-60, the Tokamak Fusion Test Reactor (TFTR),[18] and ASDEX-Upgrade[19] have also shown that pellet fueled discharges can exceed the Greenwald limit. [It is apparent the that commonly-used term "Greenwald density limit" can be a misnomer; we will use the scaling as a normalization, *i.e.,* $G_n \equiv \bar{n}_e/(I_p/\pi a^2)$, where G_n is the "Greenwald number."]

In gas-fueled, H–mode discharges a different density limit behavior has been observed[20] in DIII–D[21] and many other tokamaks. Sufficiently high neutral beam injection (NBI) triggers

an L–H confinement mode transition, at which point the line-average density ($\bar{n}_e$) increases. At the onset of type 1 edge-localized modes (ELMs), the $\bar{n}_e$ clamps at between 0.5 to $0.7*\bar{n}_e^{max}$, dependent on wall conditions. Gas puffing results in modest $\bar{n}_e$ increase followed closely by partial detachment of the divertor plasma from the target plate, which is characterized[22] by a reduction in particle and power flux and plasma pressure at the separatrix but not far into the SOL. An increase in the gas puffing rate leads eventually to total detachment at the target plate, which is characterized by a reduction in particle and power flux and plasma pressure along the entire divertor target. Energy and particle confinement is reduced during this phase, until L–mode confinement is obtained at 0.8 to $1.0*\bar{n}_e^{max}$. The H–L mode "density limit," therefore, is an operational-space limit and not a disruptive limit. As observed in the L–mode data, there is at most a very weak heating power dependence of the density limit.[20]

The density limit has recently become an important design issue[23] for the International Thermonuclear Experimental Reactor (ITER).[24] It is desirable to operate ITER at $\bar{n}_e \sim 1.3\times10^{20}$ m^{-3} ($G_n = 1.5$) with H–mode confinement for ignition margin and to ensure detachment of the divertor plasma. The confinement requirement is defined relative to ITER93H scaling[25]: $\tau_E/\tau_E^{ITER93H} \geq 0.85$.

It is notable that Greenwald scaling does not have a theoretical basis for auxiliary-heated discharges. To understand the various processes which can limit plasma density while maintaining H–mode confinement, a series of experiments was conducted on the DIII–D tokamak. We have studied the limits imposed on density by the following processes: (1) SOL/divertor thermal collapse; (2) particle confinement/fueling rate; (3) formation of a MARFE (Multifaceted Axisymmetric Radiation zone From the Edge)[26,27] on closed flux surfaces; and (4) MHD activity onset. We have used our understanding of the aforementioned processes to demonstrate the existence of an operating space with $G_n > 1$ and H–mode confinement. Our eventual goals are to understand quantitatively the mechanisms behind each limit and to determine an operational path which may be used by ITER to access this regime.

This paper is organized as follows. Section II describes the experimental approach and main tools for fueling profile control. Section III discusses the divertor power balance limit. Section IV examines particle confinement and fueling limits associated with pellet fueling. Section V details observations of MARFE formation and the relation to the density limit. Section VI describes MHD activity observations. Section VII shows the proof-of-principle high density discharges with H–mode confinement, after avoiding each of the other limits. A summary and conclusions are given in Section VIII.

II. APPROACH

Our operating premise was that the H–L density ''limit'' was caused by SOL or divertor thermal collapse, described, for example, by the Borass density limit.[6] We postulated that this limit could be avoided by density profile control, which is achievable by simultaneous use of direct core pellet fueling and divertor pumping. Past operational experience has shown that use of gas puffing to increase $\bar{n}_e$ also increases the electron density at the magnetic separatrix in the main chamber. The divertor electron density has been shown[28] to increase non-linearly with the main chamber separatrix density and the divertor temperature decreases non-linearly; this dependence can lead to a thermal collapse when the density gets sufficiently high. By fueling inside the separatrix with pellets and using divertor pumping, we sought to maintain the edge density below the level at which the thermal collapse would occur. The other benefit of divertor pumping is to reduce neutral pressure buildup in the divertor, thereby reducing hydrogenic radiation.

The present pellet injector[29] on the DIII–D tokamak is capable of injecting three different diameter pellets: 1.8, 2.7, and 4.0 mm at maximum, programmable injection frequencies of 10, 10, and 5 Hz, respectively. For the discharges studied in this experiment, the ratio of the particle content of the pellets to the plasma content was 5% to 15% (1.8 mm), 15% to 45% (2.7 mm), and 50% to 150% (4.0 mm), depending on the plasma density. The DIII–D cryopump is a cryogenic condensation pump[30] with a pumping speed ~ 30 m^3/s at 1 mTorr plenum pressure. The plenum pressure buildup and the particle exhaust rate (pumping speed times plenum pressure) can be varied by movement of the outer divertor strike point relative to the pump plenum entrance.

III. DIVERTOR COLLAPSE/DETACHMENT AND H–MODE CONFINEMENT LIMIT

The phenomenology of H–mode density limit discharges is discussed in detail in this section (see also Ref. 20). The time dependence of a pellet-fueled density limit discharge is shown in Fig. 1 (solid curves). The L–H transition occurs prior to $t = 2$ s and is not shown; 2.7 mm pellets are injected every 200 ms starting at $t = 2.6$ s and cause transient $\bar{n}_e$ increases [Fig. 1(a)]. The first pellet causes the formation of a high density, high radiation zone in the divertor plasma. We will refer to this zone as a "divertor MARFE"; migration of the zone onto closed flux surfaces leads to a MARFE in the classic sense and we will drop the "divertor" adjective in those cases. The sharp increase in the outer divertor D_α baseline at $t = 2.6$ s is one signature of the divertor MARFE [Fig. (1b)]. Note that the outer divertor target density [measured by a Langmuir probe — Fig. 1(c)] began to roll over after the second pellet. Between 2.6 and 3.5 s, the divertor MARFE gradually moved from the open field lines in the scrape-off layer (SOL) to the X–point area, near closed-field lines. This motion was observed in 2-D reconstructions of the radiation distribution from bolometry. Concomitant with the density roll over and divertor MARFE migration was a decrease in the energy confinement time [Fig. 1(d)]. Note that both $\bar{n}_e$, radiated power, and D_α baseline continued to increase during this phase [Fig. 1(a),(c),(d)]. The divertor plasma completely detached from the target at $t = 3.5$ s [rollover of D_α in Fig. 1(c)], and the energy confinement time dropped back to L–mode levels. At this point, the $\bar{n}_e$ rolled over and further increase in $\bar{n}_e$ could not be achieved.

In contrast, Fig. 1 also shows a discharge (dashed) in which the divertor cryopump was activated. While the initial $\bar{n}_e$ and divertor density were lower in the pumped discharge than the unpumped discharge, the peak values were comparable [Fig. 1(a),(c)]. Note that the radiated power was reduced by pumping [Fig. 1(d)], which prevented the divertor detachment/collapse phase observed in the unpumped discharge. A divertor MARFE was formed after each pellet in the pumped discharge, but it disappeared in the time between pellets. Thus migration of the divertor MARFE to the X–point region was avoided, as was the energy confinement degradation [Fig. 1(e)], which always accompanies divertor MARFE migration to closed flux surfaces. Further experiments are required to quantify the mechanism which prevents divertor MARFE sustenance and migration, but it is probable that the reduction of the private flux region neutral pressure [Fig. 1(f)], which has been proposed[31] as a key control parameter, plays a role. The fact that the divertor density was comparable in these two discharges suggests that the divertor density is not at a limiting value. In the pumped discharge, the minimum exhaust rate to prevent divertor MARFE sustenance was used. Increasing the pumping rate by changing the geometry would have been counter-productive because it would have reduced the particle containment time τ_p^* which would increase the fueling rate required to reach high density.

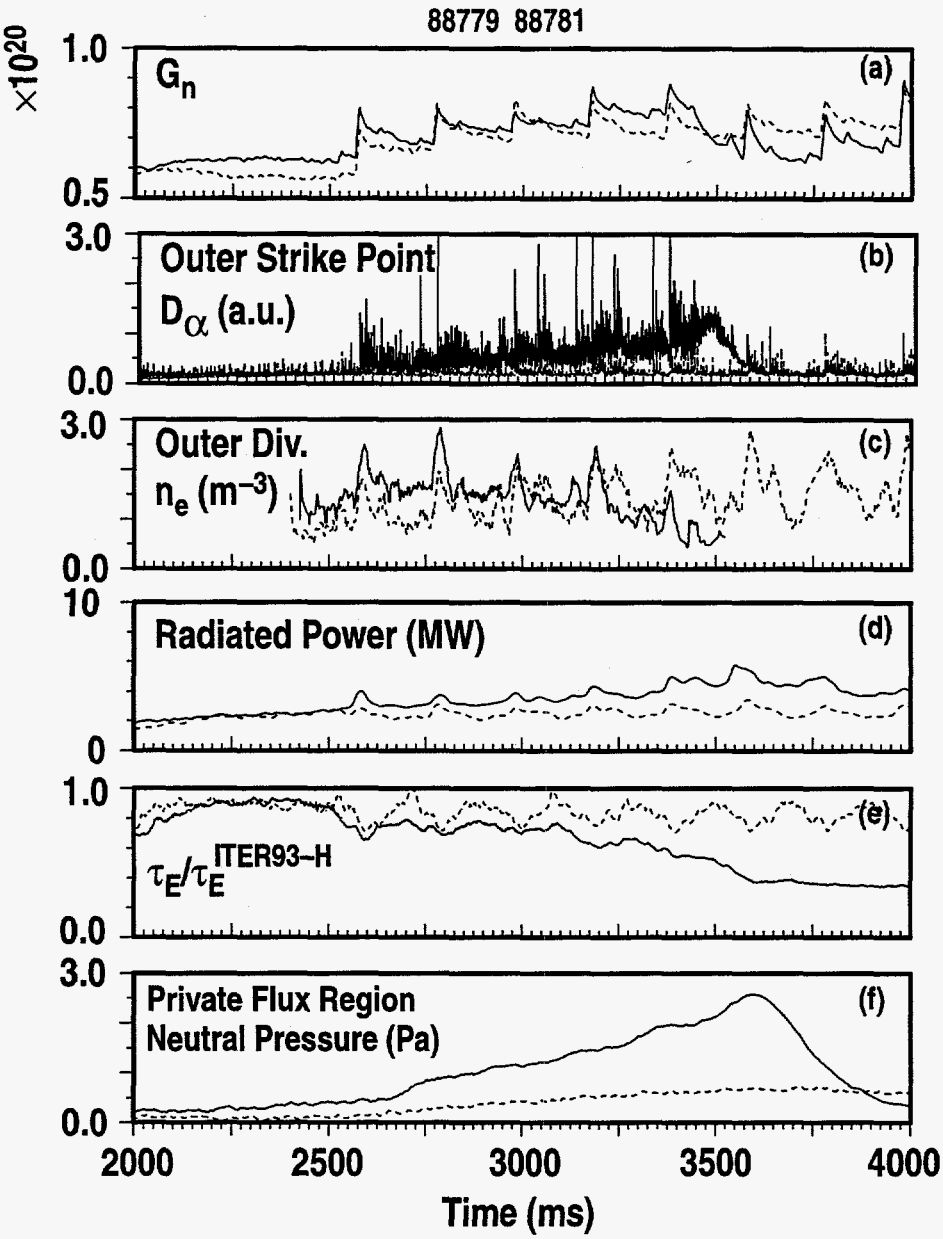

Fig. 1. H–L density "limit" and divertor thermal collapse were avoided by activation of the cryopump (dashed). Both discharges had $I_p = 1.3$ MA and NBI power ~5 MW; pellet injection was initiated at $t = 2.6$ s. (a) G_n was comparable in both discharges. (b) Outer strike point D_α emission increased sharply after pellet at $t = 2.6$ s and stayed high between pellets. The grassy character of the D_α is a signature of a divertor MARFE for the unpumped discharge. Pumping prevented a sustained divertor MARFE. (c) Electron density at the target rolled over for unpumped discharge. Peak divertor density was comparable for pumped and unpumped discharges, but pumping reduced density between pellets. (d) Confinement degradation was avoided in the pumped discharge. (e) Radiated power was reduced in the pumped discharge. (f) Private flux region neutral pressure was reduced in pumped discharge.

IV. PARTICLE CONFINEMENT AND FUELING LIMITS

Another mechanism which can limit plasma operating density is poor particle confinement time and/or poor fueling efficiency. The importance of these two effects can be discussed by considering the main plasma particle balance equation:

$$\frac{d}{dt}\left(\bar{n}_e V_p\right) = S_p(t) - \frac{\bar{n}_e V_p}{\tau_p^*}, \tag{1}$$

where V_p is the plasma volume, S_p is the particle source term, and τ_p^* is the effective particle containment time, including the effects of recycling. Here it is implicitly assumed that $\bar{n}_e$ can be used as an approximation for the volume-averaged density. In steady-state with a steady source term, $\bar{n}_e = S_p \tau_p^* / V_p$. Consider a perturbation to the equilibrium density with pellet injection at a fixed pellet size N_{pel}, frequency ν_{pel}, and fueling efficiency η_{pel}. Each pellet increases the density by $\eta_{pel} N_{pel}/V_p$, and the density in excess of the pre-pellet H–mode density decays away exponentially with a decay time, τ_n. This τ_n is distinct from the recycling-dominated particle containment time τ_p^* because of the difference in the fueling source profile. The density decay rate from the main plasma between pellets increases with the density; in steady state, the decay between pellets balances the density increase after each pellet, $\eta_{pel} N_{pel}/V_p$. The solution for the total density rise after the m^{th} pellet just before the $m+1^{st}$ pellet in steady state relative to Greenwald scaling ΔG_n is given by:

$$\Delta G_n = \frac{\eta_{pel} N_{pel}/V_p}{I_p/\pi a^2} * \left[\frac{1}{1-\exp\left(-1/\tau_n \nu_{pel}\right)} - 1\right], \tag{2}$$

Above, m is the number of pellets large enough to achieve steady state. Equation (2) shows that the dependence of ΔG_n on $\tau_n \nu_{pel}$ is quite strong: for $\tau_n \nu_{pel} = 1$, the term in brackets is $1/(e-1) \sim 0.58$ and falls to ~ 0.16 for $\tau_n \nu_{pel} = 0.5$. Equation (2) also indicates that the ΔG_n is linearly proportional to η_{pel} and always increases with the ν_{pel}, provided τ_n is independent of ν_{pel}. Thus, ΔG_n is always dependent on the fueling rate. With fixed fueling parameters, however, we will show that ΔG_n can also be dependent on I_p because of the scaling of τ_n with I_p.

A. Plasma current dependence

The I_p dependence of ΔG_n can be examined by assuming $\tau_n \propto I_p^\alpha$ for different α, where $\alpha = 1$ corresponds approximately to the measured dependence of the energy confinement time[32] in DIII–D. A calculation for a DIII–D sized plasma and 2.7 mm pellets is plotted in Fig. 2. For simplicity, we have used $\eta_{pel} = 1$, $N_{pel} = 9.3e20$ atoms (2.7 mm pellet),

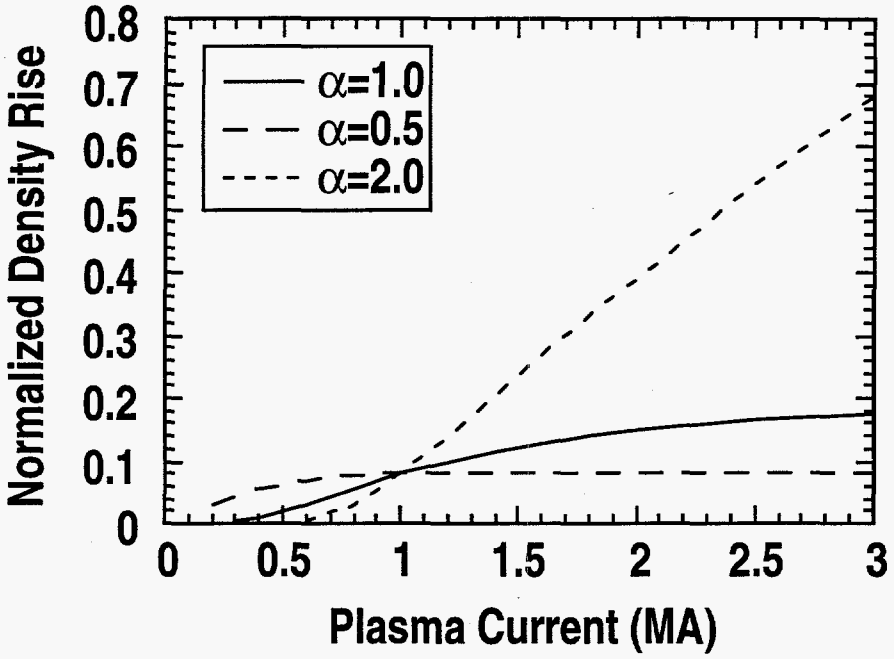

Fig 2. Calculation of expected density rise from periodic pellet injection ΔG_n versus I_p from Eq. (2), assuming for $\tau_n \propto I_p^{\alpha}$. For $\alpha = 2$, note that ΔG_n always increases with I_p.

$V_p = 20\ m^3$, $\nu_{pel} = 10$ Hz, and $\tau_n[s] = 0.05 * I_p^{\alpha}[MA]$. The constant 0.05 is obtained from measured decay times, discussed below. The features of the solution for $\alpha = 1$ are: (1) for $I_p < 1$ ($\tau_n \nu_{pel} < 0.5$), ΔG_n increases strongly with I_p (I_p dependent regime); and (2) for $I_p > 2$ ($\tau_n \nu_{pel} > 1$) ΔG_n increases weakly with I_p (I_p independent regime). For $\alpha > 1$, it is seen that ΔG_n is always I_p dependent . In the I_p dependent regime, increasing ΔG_n by raising I_p should be more effective than increasing the fueling rate because experimental evidence has indicated that increasing the fueling rate can decrease the energy and particle confinement times, *i.e.*, the two are not completely independent.

Here it should be mentioned again that Greenwald's conclusion of the gas-fueled density limit was that the particle confinement time decreased rapidly above $G_n \sim 1$. The variation in G_n on Alcator-C was accomplished[1] partly by reducing I_p at constant $\bar{n}_e$ (as opposed to increasing $\bar{n}_e$ at constant I_p). This technique, however, can mask any non-linear dependence of τ_n on I_p. To examine this, we varied G_n and I_p independently on DIII–D by injecting both 2.7 and 4.0 mm pellets into discharges at different I_p levels and measuring the pellet density decay times. The density just before each pellet was injected was subtracted as a baseline in the fits. We have restricted our dataset to ELMy discharges with NBI power between 5.5 and 8 MW at a toroidal field (B_t) of 2.1 T. Figure 3 demonstrates that there is at most a weak decline of τ_n with G_n at $I_p = 0.7$ and 1.3 MA. Therefore, our data is inconsistent with Greenwald's conclusion that particle confinement decreases catastrophically near $G_n = 1$. Note that there is factor of 2-3 variation in the dataset at each I_p. Nonetheless, it is shown that the average τ_n for the 1.3 MA data is 3 to 5 times larger than for the 0.7 MA

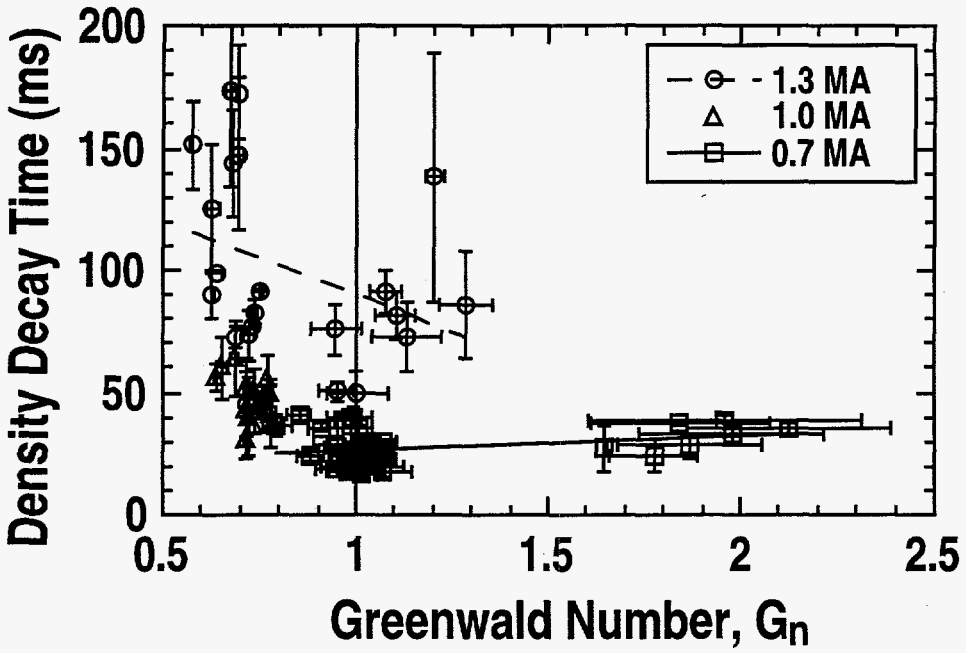

Fig 3. Measured τ_n is largely independent of G_n but increases nonlinearly with I_p.

data and about 60% higher than the 1.0 MA data. Fitted to a power law dependence, $\tau_n \propto I_p^2$. Thus we conclude that Greenwald's observations of τ_n decreasing sharply for $G_n > 1$ may have been caused largely by a non-linear dependence of τ_n on I_p. Our calculations in the previous section, thus, imply that obtaining $G_n > 1$ with pellet fueling would be done most easily at high I_p because the $\tau_n \propto I_p^2$ insures operation in the I_p dependent regime. It is noteworthy that q was varied along with I_p in this dataset; therefore, a separate dependence of τ_n on q cannot be ruled out.

One additional point should be made: on DIII–D, it has been observed that the density in gas-fueled, ELMy H–mode plasmas clamps to an integer multiple of I_p.[32] The inference from those observations is that $\tau_p^* \propto I_p$. In contrast, our pellet fueling results indicate $\tau_n \propto I_p^2$. We hypothesize that the different scalings may be due to the difference between recycling-dominated shallow fueling, and the pellet-dominated deep fueling into the highest confinement region. In other words, there may be a fundamental difference in the dependence of τ_p^* and τ_n on plasma current.

B. Fueling efficiency limits

Equation (2) indicates the importance of the fueling efficiency in increasing density. For reference purposes, gas-fueled discharges typically have a fueling efficiency of $\leq 10\%$. Pellet-fueled discharges can have a much higher fueling efficiency, up to 100%. Pellet penetration in general has been shown[33] to be dependent on the electron temperature profile and the fast ion content, both of which increase with the NBI power level. Figure 4 shows

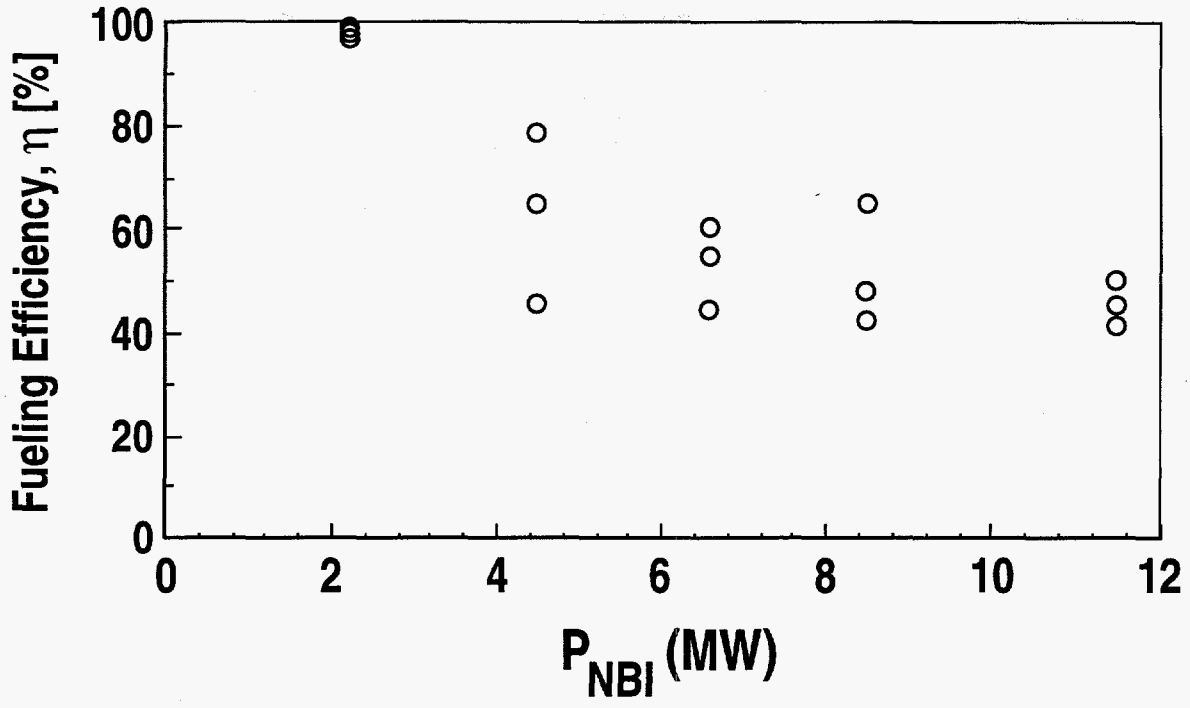

Fig. 4. Measured penetration depth of 1.8 and 2.7 mm pellets increases with decreasing T_e at $\rho = 0.3$.

that the pellet fueling efficiency η, defined as the fraction of pellet atoms appearing in the plasma just after injection, does decrease with the NBI power. Pellet fueling studies[18] in ELMy H–mode plasmas on the ASDEX-Upgrade tokamak have shown that the pellet net fueling efficiency can decrease to $< 20\%$ if pellets fail to penetrate beyond the ELM depth region. Thus the highest attained densities in our experiment occurred when the target electron temperature was sufficiently low to allow penetration beyond the ELM depth layer. There is a synergistic effect here: a pellet which penetrates deep into the plasma increases the density, causing a proportional decrease in temperature (the fueling process is approximately adiabatic); the succeeding pellets therefore have even deeper penetration and thus higher fueling efficiencies. To achieve and maintain low temperatures, the NBI power was usually programmed to ≤ 5 MW during the first few pellets. Attempts were made to increase the NBI power as the density increased, but MHD activity was often observed (discussed in the MHD section). Thus the heating power appeared to have an upper (MHD) limit ~ 3 MW in many cases, and the highest density discharges actually had input power ≤ 2 times the threshold power required for the L–H transition.

An interesting phenomenon in these low NBI power discharges was observed — often the density decay time following pellet injection was reduced down to ~ 5 ms. By examining the edge density, temperature, and pressure profiles and gradients, it was determined that H–L transitions were often induced by the pellets. Figure 5 shows such a transition: the density at the H–mode edge pedestal decreases, magnetic fluctuations and divertor D_α

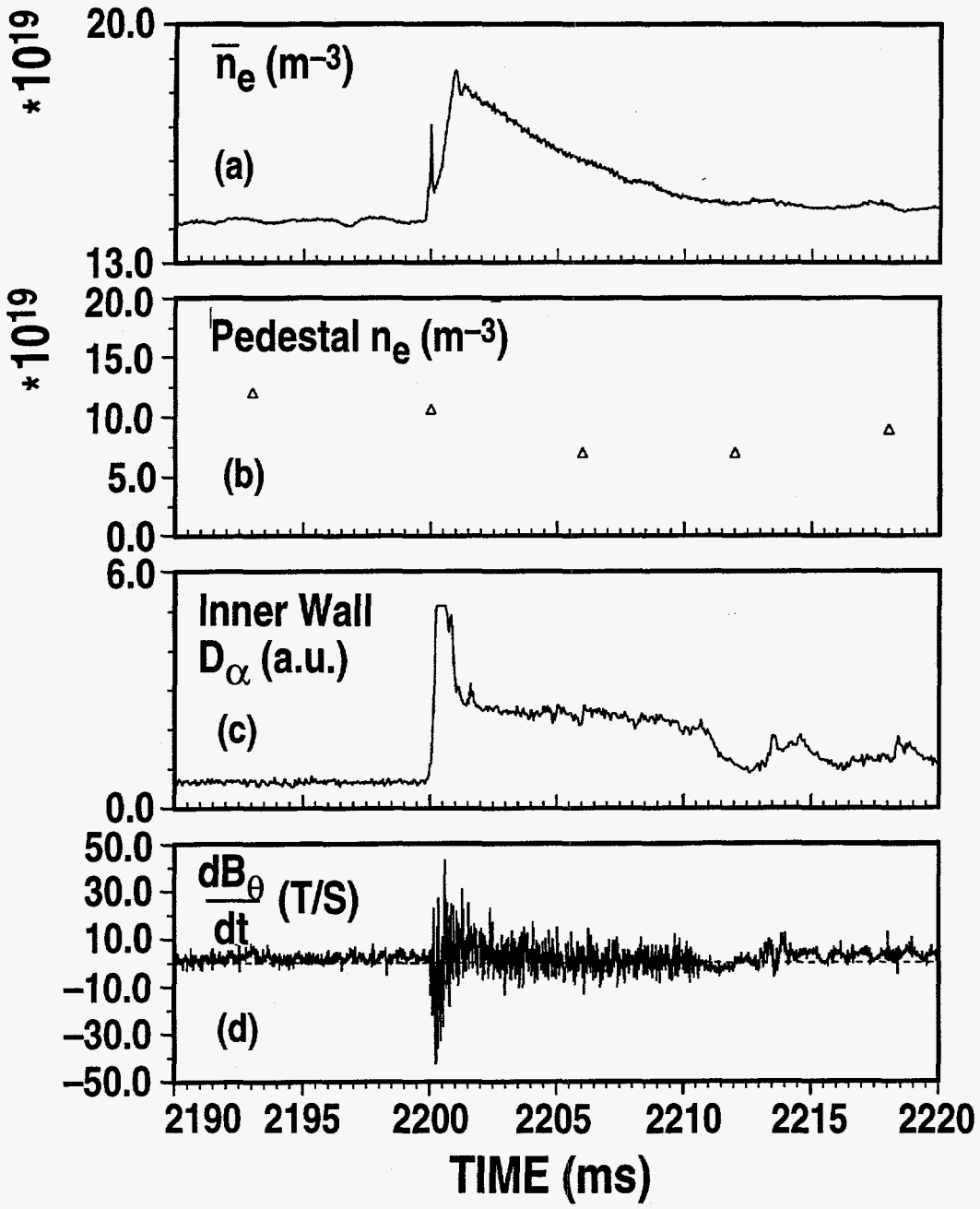

Fig. 5. Example of a pellet-induced H–L transition of ~11 ms duration. (a) $\bar{n}_e$ decreases rapidly after pellet at $t = 2200$ ms. (b) Edge pedestal n_e is reduced and starts to re-build after ~15 ms. (c) centerpost D_α increases at time of pellet injection and stays at L–mode levels for ~11 ms. (d) dB_θ / dT from a magnetic probe indicates enhanced fluctuations for ~11 ms.

increase, and $\bar{n}_e$ decays rapidly. The pellet retention fraction, defined as the fraction of the initial pellet density rise which is retained in the plasma at the end of the L–mode duration, is plotted as a function of the L–mode duration in Fig. 6. The data show that the pellet retention fraction decreases sharply with the L–mode duration with a density decay time of 5 ms.

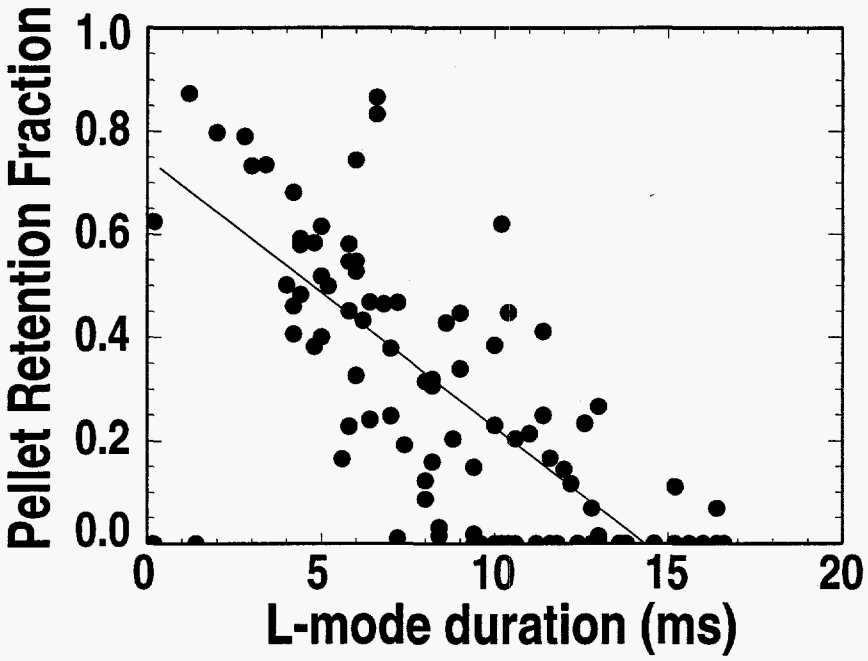

Fig. 6. Pellet retention fraction, defined as the fraction of the initial pellet-induced $\bar{n}_e$ rise present in the plasma at the end of the L–mode duration, decreases rapidly with increasing L–mode duration. Dataset had $I_p = 1.3$ MA and P_{NBI} between 2.5 and 4 MW.

Since this effect appears to be related to the H–mode power threshold, then the presently accepted H–mode power threshold scaling for DIII–D indicates[34] that decreasing the toroidal field (B_t) would give more margin over the power threshold. The duration of the L–mode phase is plotted as a function of B_t in Fig. 7 for discharges with the same I_p and roughly the same NBI power. Note that both the average and maximum observed L–mode duration following pellets increased with B_t, implying that the observed effect is consistent with H–mode power threshold scaling. The scatter in the data may be related to differences in individual pellets and other hidden variables.

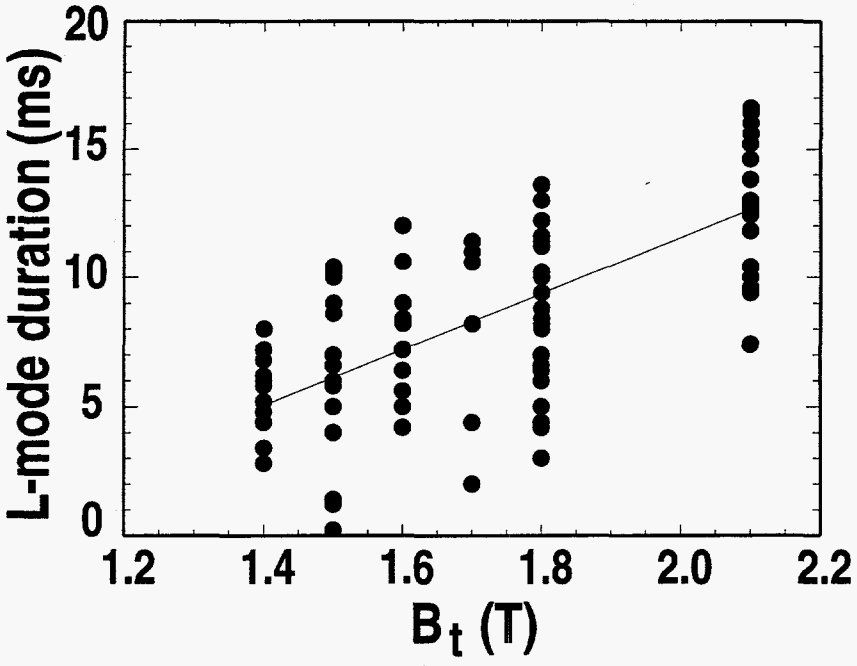

Fig. 7. L–mode duration increases with toroidal field B_t for the same dataset in Fig. 6.

V. MARFE ONSET

MARFEs can limit density in the following way. A density rise in a discharge with a MARFE causes a rapid increase in the MARFE density and radiated power,[20] which can lead to a global thermal instability and subsequent current channel contraction and MHD instability. The resulting reduction in edge temperature can lead to current profile shrinkage and MHD instability. As discussed above, the typical unpumped DIII–D density limit disruption involves migration of a divertor MARFE from the SOL to the X–point region and then onto closed flux surfaces. This edge/divertor collapse limit was avoided by divertor pumping (Section 3). Note that divertor MARFE formation just after pellets was not prevented, but that the divertor MARFEs were pumped out between pellets.

Theories of MARFE formation on closed field lines balance parallel and radial heat flow with radiative losses. These theories[35,36] show that MARFEs should form most easily during high q_{95} discharges. To test MARFE formation and stability, two discharges with a three-fold q_{95} variation were executed. Figure 8 shows that a MARFE formed at the inner wall midplane for the high q_{95} discharge at $G_n \sim 0.8$. In comparison is a low q_{95} discharge which achieves $G_n \sim 2$ and is free of MARFE formation. Thus it is clear that MARFE formation can be made independent of G_n .

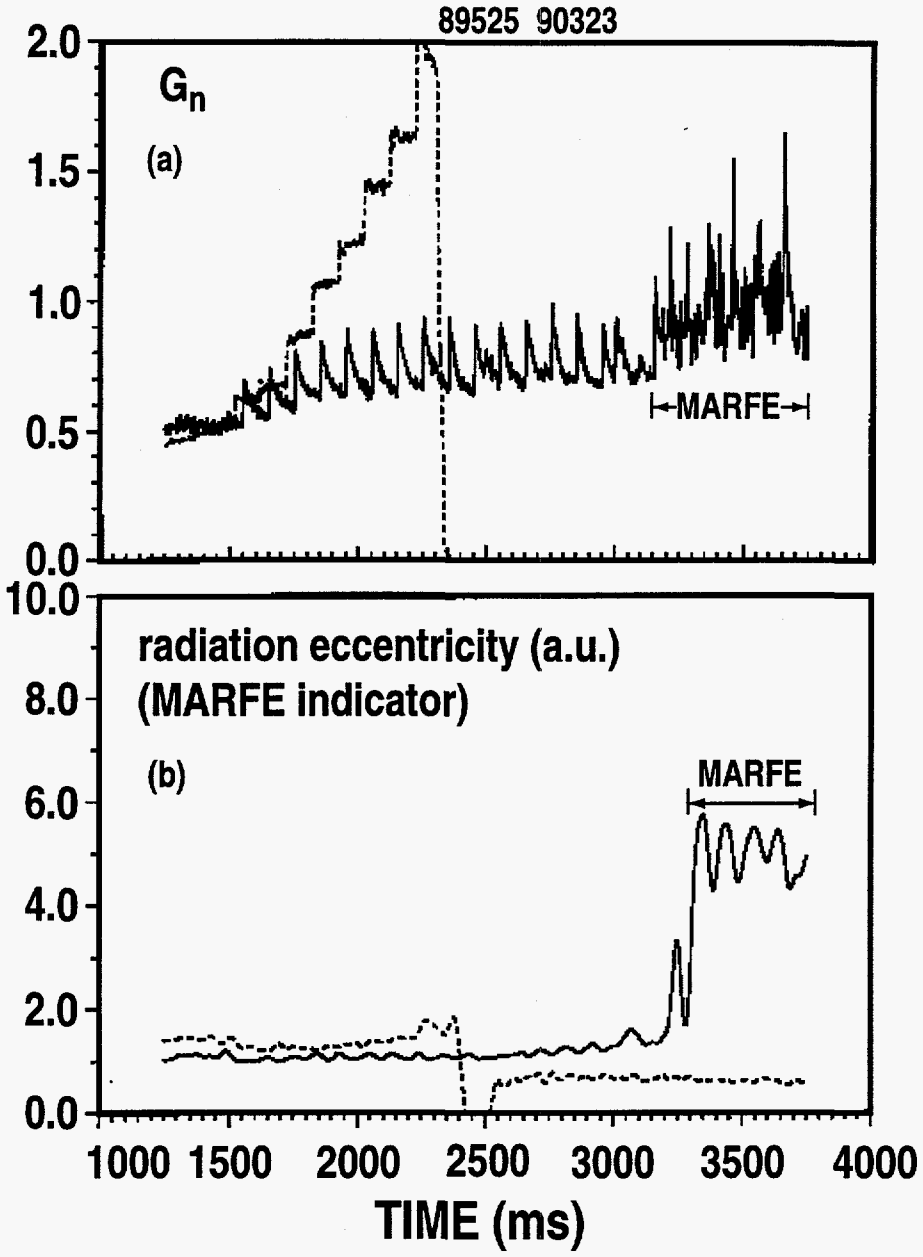

Fig. 8. MARFE observed during high q operation (solid) and avoided by low q operation (dashed). (a) G_n ($\bar{n}_e$ measured by a chord looking across the plasma midplane) observes a perturbation $t = 3200$ ms. (b) radiation eccentricity, defined as ratio of inner wall bolometer chord signal to an unaffected (non-divertor) chord signal, increases at $t = 3250$ ms, indicating presence of inner wall MARFE.

VI. MHD ACTIVITY

As discussed above, the final phase of a density limit disruption is characterized by the growth of a low m,n tearing-type mode, usually the 2/1. The mode appears and locks some time after the H–L transition, resulting in a disruption or rapid stored energy ejection. The growth of these modes and their impact on confinement is usually larger for low edge safety factor (q_{95}) discharges than high q_{95} discharges. In our experiments, these modes were often observed as pellets were used to increase the density over a wide range: $0.7 < G_n < 1.5$. For an adiabatic $\bar{n}_e$ increase, the electron temperature and toroidal rotation decrease proportionally, making high density discharges potentially more vulnerable to locked modes.

Fourier analysis of Mirnov oscillations has been done to identify the mode structure of MHD activity in our discharges. Figure 9 shows the onset of a $m/n = 3/2$ tearing mode, occurring just after the injected pellet at $t = 1.9$ s. The amplitude of the mode grows to ~ 6 G and is then reduced as safety factor on axis (q_0) increases. The disappearance of the mode coincides with q_0 increasing above 1.5. We have computed the island growth rate parameter,[37] Δ' at the $q = 1.5$ surface from a magnetically reconstructed equilibrium [Fig. 9(d)]. Details of the technique used to estimate Δ' have been discussed previously.[38] Our estimates indicate that $\Delta'_{3/2} < 0$ just before onset of the mode. Neglecting neoclassical effects at this high density/ collisionality, the plasma should be stable against growth of the mode, which is inconsistent with the observations. The 3/2 mode in this case has a negligible impact on the energy confinement. Tearing modes with $m/n = 2/1$ have also been observed — these modes sometimes lock and have a large impact on confinement. Figure 10 compares two discharges — the only operational difference is that 600 kW of extra beam power was added at $t = 2$ s in the dashed discharge. In the higher power discharge, the 2/1 mode is de-stabilized just after $t = 2$ s and locks at $t = 2.12$ s [Fig. 10(c)]. Particles and energy are rapidly expelled after locking of the mode. Our calculations indicate that $\Delta'_{2/1} < 0$ just before onset of the mode [Fig. 10(d)], indicating stability to classical tearing modes. Recent beta limit studies of gas-fueled discharges[39] with a similar shape and configuration obtained a beta limit at normalized beta [$\beta_N \equiv /(I_p/aB_t)$] ~ 4, in quantitative agreement with the theory of neoclassical destabilization of tearing modes. The discharges in this section have much higher density and collisionality, thereby reducing the predicted magnitude of neoclassical effects. Thus it is unclear why MHD activity was encountered for these higher density, lower $\beta_N \sim 1.4 - 1.5$ discharges. Note that our dataset is too small to conclude that the onset of MHD activity is encountered at a critical beta value at high density. However it is noteworthy that the 2/1 mode was not observed at $G_n > 1$ when the NBI power < 3 MW.

We conjecture that the MHD activity may be caused by the triggering of "snakes" by pellets. Snakes have been observed[40] on JET with pellet injection, typically when pellets penetrated to

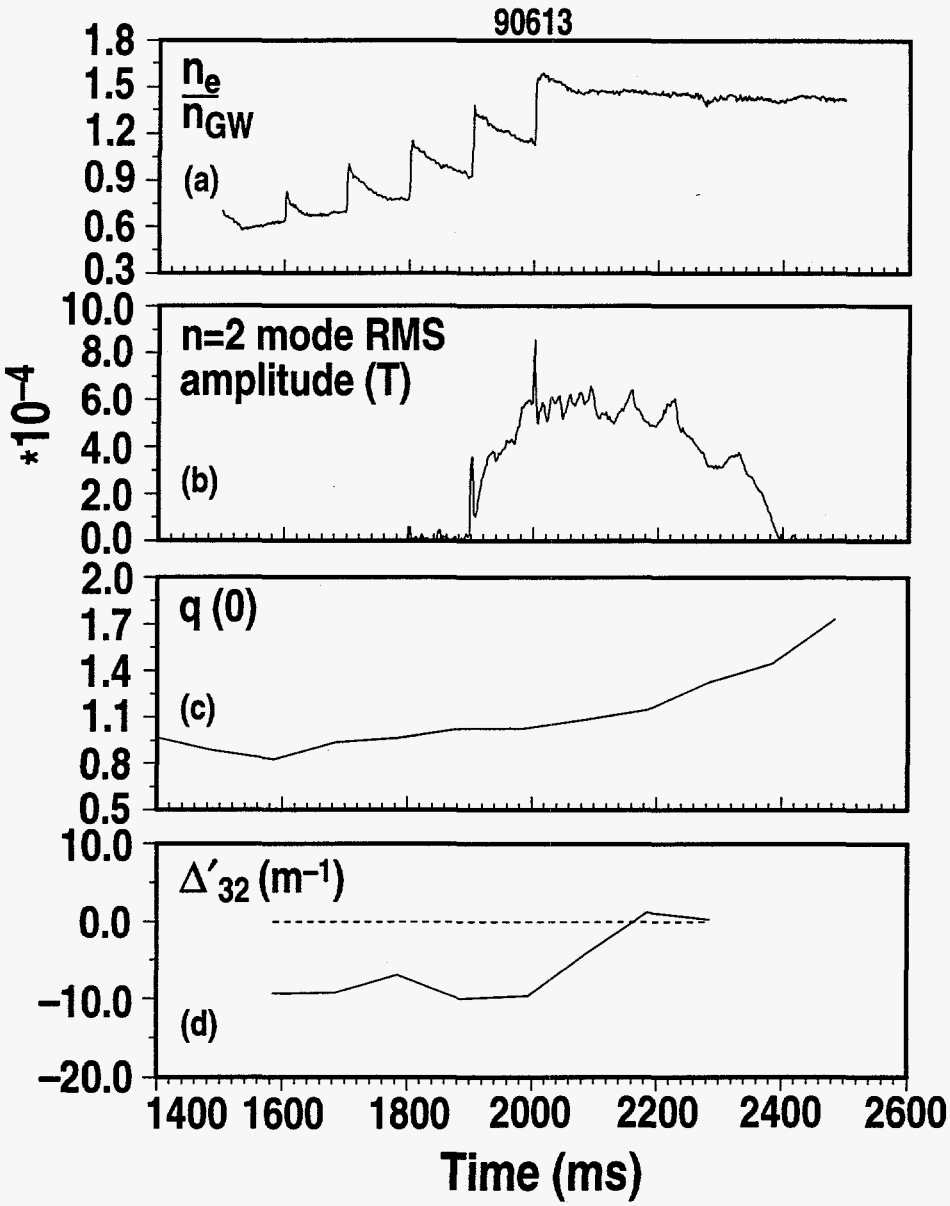

Fig 9. Destabilization of $m,n = 3/2$ mode for a pellet-fueled discharge. (a) G_n increased as pellets were injected. (b) MHD mode with $m,n = 3/2$ was destabilized at $t = 1900$ ms, almost coincident with pellet. (c) q on axis from equilibrium reconstruction. The 3/2 mode disappears when $q(0)$ exceeds 1.5, as expected. (d) Δ' calculated at $q = 1.5$ from reconstructed equilibrium is < 0 for $t < 2100$ ms, indicating theoretical stability to classical tearing mode onset.

the $q = 1$ surface. Snakes appear as oscillations in the 2D reconstruction of soft x–ray (SXR) emission patterns. Snakes are believed[41] to originate from pellet deposition at rational surfaces. The thermal capacity of flux tubes intersecting pellet trajectories on rational surfaces is low compared with the entire flux surface. Even nominal pellet ablation within such a flux tube could lead to a rapid local temperature drop. This local temperature drop would lead to a

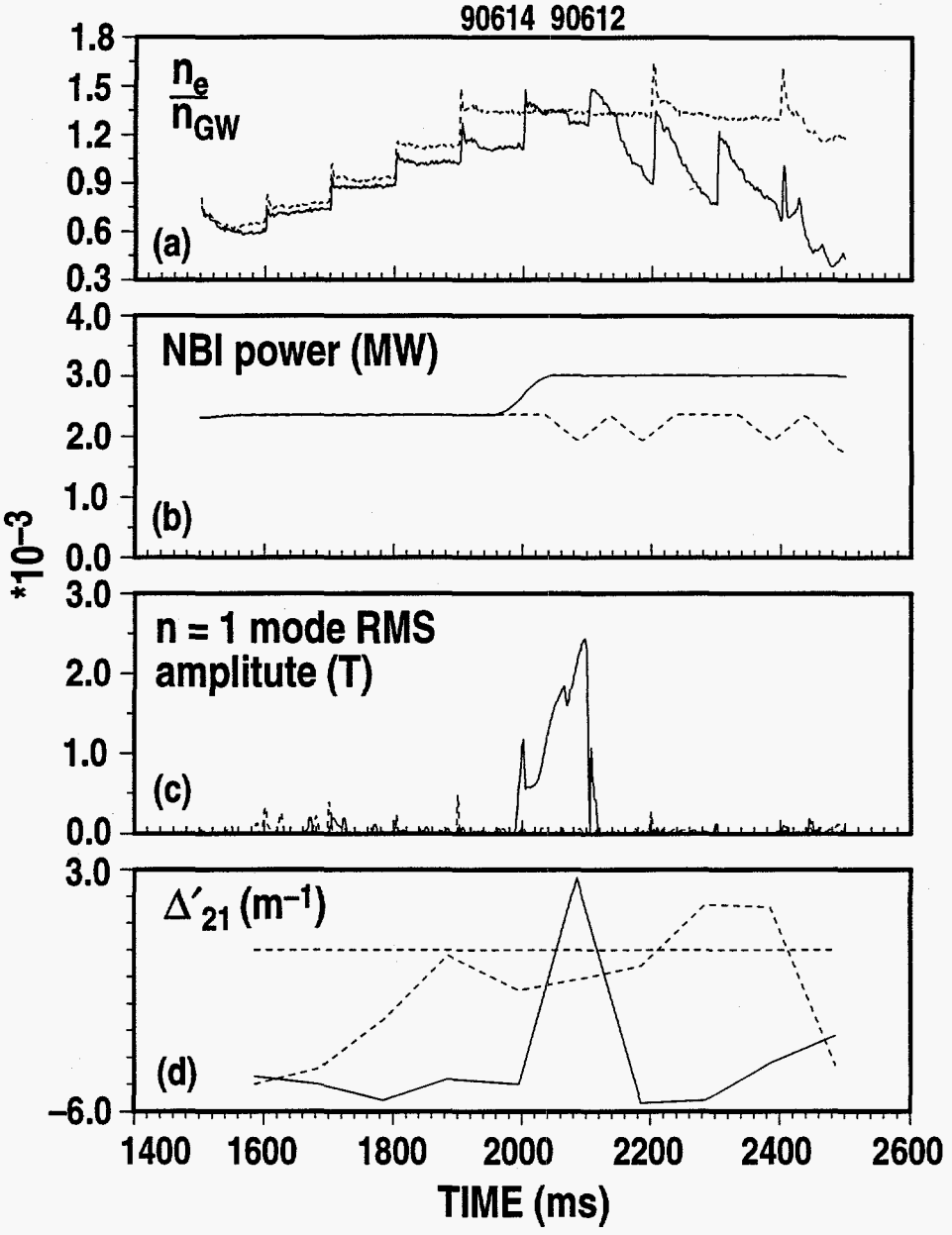

Fig. 10. Increase in NBI power correlated with destabilization of 2/1 mode for pellet-fueled discharges. (a) G_n increased as pellets were injected into both discharges. (b) NBI power increased at $t = 2000$ ms (solid). (c) MHD mode with $m,n = 1/2$ was destabilized at $t = 2100$ ms, almost coincident with pellet (solid). Lower power discharge (dashed) is stable. (d) Δ' calculated at $q = 2$ from reconstructed equilibrium is < 0 at $t = 1990$ ms, indicating theoretical stability to classical tearing mode onset for both discharges.

local resistivity enhancement, which can be a destabilizing term in the island growth rate equation.[41] Most of the injected pellets did not penetrate to the $q = 1$ surfaces in our discharges, but similar instabilities could be triggered, in principle, by pellet penetration to the $q = 1.5$ or $q = 2$ surfaces. We could not see direct evidence of snakes, however, because the

central temperature of the discharges in Figs. 9 and 10 was below the lower cutoff of the present SXR system.

VII. DEMONSTRATION DISCHARGE WITH G_n ~ 1.5 AND H–MODE CONFINEMENT

As previously mentioned, it is desirable to operate ITER at $G_n \sim 1.5$ with H–mode confinement. After evaluating the various processes detailed above, we optimized conditions to demonstrate $G_n \sim 1.5$ with H-mode confinement.. The edge/divertor collapse limit merely required operation of the divertor cryopump. The non-linear increase of the density decay time with I_p called for high current operation; the upper limit on I_p was set by the volt-second consumption rate. The MHD limits, though not well understood, were avoided at low NBI power; this was also optimum for pellet penetration and fueling efficiency. At high density and in light of the MHD-induced NBI limit, the occurrence of pellet-induced H–L transitions required reduction of B_t from the maximum value of 2.1 to ≤ 1.5 T. And finally the core MARFE limit was avoided by low q_{95} operation, which is consistent with high I_p and low B_t.

One of these discharges is shown in Fig. 11. A pellet interlock scheme was developed and utilized to prevent injection above a specified G_n, in this case $G_n \sim 1.5$. Thus, pellet injection was interlocked after $t = 2.0$ s and $G_n \sim 1.5$ was maintained from 2.0 to 2.6 s. However, the radiated power and energy confinement were evolving during the steady density phase [Fig. 11(b),(c)]. The energy confinement time peaked at ~ 1*ITER93-H scaling, and stayed above 0.75*ITER93-H scaling for 300 ms. Note that during the density rise phase from 1500–2000 ms, ELM activity was observed [sharp spikes in divertor D_α emission — Fig. 11(d)]. However after the pellet at $t = 2000$ ms, ELM activity ceased. During the ELM-free phase, the radiated power increased, resulting in a reduction in the stored energy and energy confinement time. Spectroscopic data showed a gradual increase (not displayed) in the carbon and metallic radiation from the core during the flat-top, suggesting impurity accumulation was occurring (impurity accumulation in ELM-free discharges has been reported previously[42]). A spontaneous H–L transition was observed near the end of the density flat-top at $t = 2570$ ms, and the final pellet at $t = 2600$ ms triggered a locked mode, causing a rapid ejection of particles and energy.

It is worth mentioning that the relatively high confinement time obtained in this discharge does not result from the triggering of a pellet enhanced performance, or PEP, mode. PEP modes are characterized[43] by highly peaked density profiles and strong central heating, neither of which are present in this discharge. The density profile is highly peaked for 100 ms following the pellet at $t = 2000$ ms, but it then relaxes to a ''moderately peaked'' level later in the density flat-top phase (Fig. 12). Moreover, the NBI heating profile is extremely hollow at the obtained $\bar{n}_e \sim 1.7 - 1.8 \times 10^{20}$ m^{-3}, and the central heating rate is actually exceeded by the radiative cooling rate from 2300–2600 ms.

Time-dependent MIST modeling[44] has been done for this discharge. The impurity concentration was constrained by measured UV emission from a spectrometer, and the impurity

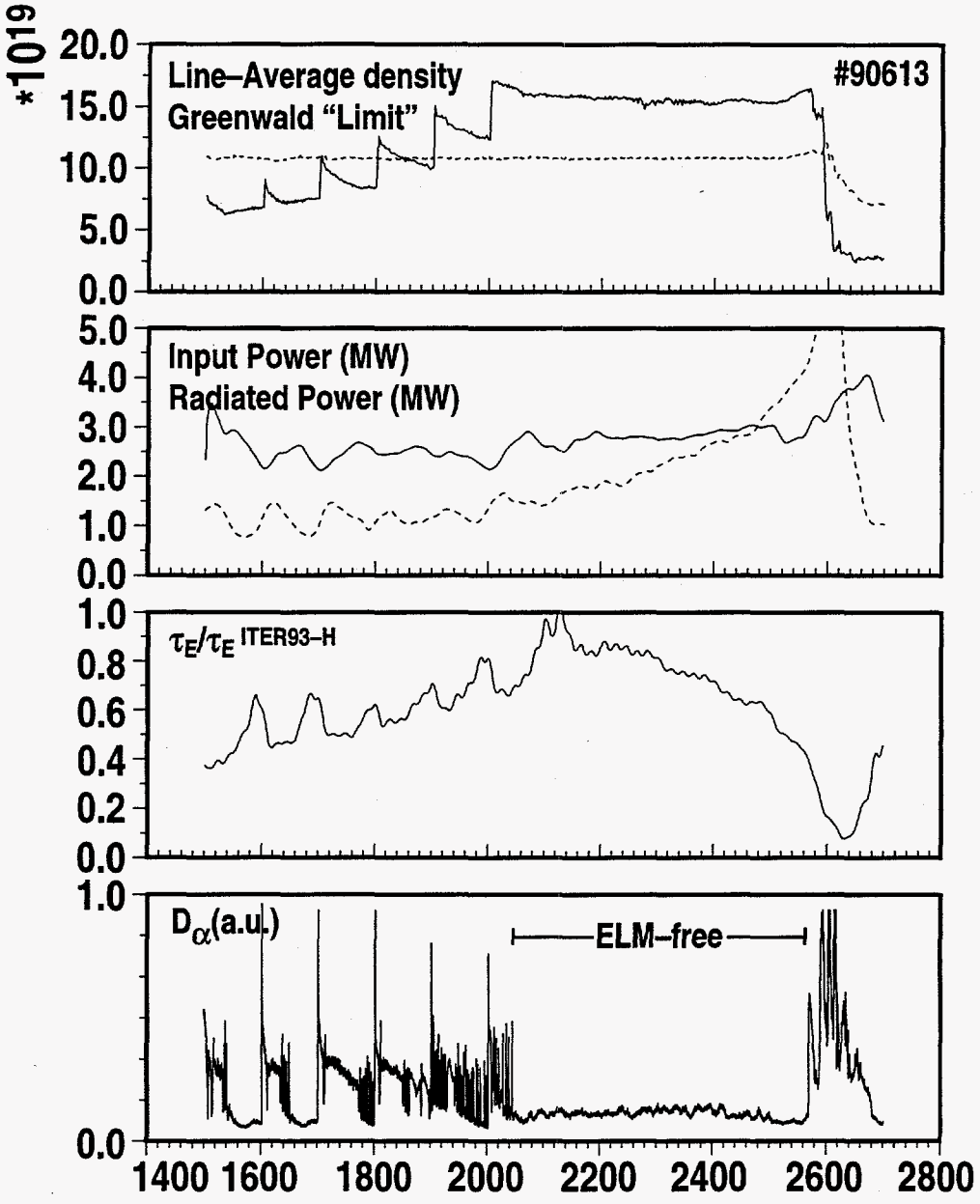

Fig. 11. Demonstration discharge with $G_n \sim 1.5$ and H–mode confinement; $I_p = 1.3$ MA, $B_t = 1.5$ T, $q_{95} = 3.2$. (a) Pellets increased $\bar{n}_e$ (solid) above Greenwald density "limit" (dashed) up to $G_n \sim 1.5$ for 600 ms. (b) Radiated power increased during density flat-top from $t = 2000$ to 2600 ms, exceeding NBI plus Ohmic power at $t = 2500$ ms. (c) Energy confinement increased during early phase of density flat-top up to $\tau_E/\tau_E^{ITER93H} \sim 1.0$ and decreased as radiation increases. (d) Divertor D_α increased as pellets were injected and ELMs were observed. From $t = 2040$ ms to 2600 ms, ELM activity ceased.

density profiles were assumed to have the same shape as the electron density profiles. The modeling shows that the impurity concentration increased during the ELM-free phase [Fig. 13(a)] and that most of the increase in radiated power came from carbon radiation inside

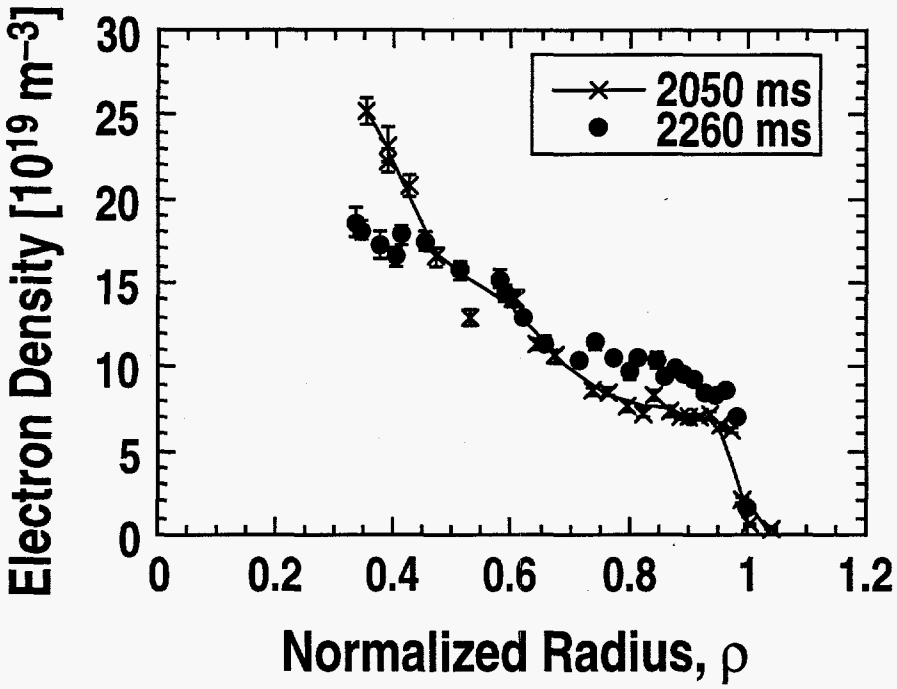

Fig. 12. Comparison of electron density profiles at $t = 2050$ ms and $t = 2260$ ms after pellet at $t = 2000$ ms for demonstration discharge in Fig. 11. Large profile peaking persists until $t = 2100$ ms but then relaxes from 2100–2600 ms.

$r/a < 0.6$ [Fig. 13(c),(d)]. At the measured central electron temperature of 400 eV, 0.5% of the carbon was calculated to be in the 5+ charge state, leading to high recombination and line radiation rates from the core. The measured central radiation emissivity from bolometry was $\sim 2.3 \times 10^6$ W/m^3 [Fig. 13(d)]; a calculation of NBI penetration yielded a central deposition source of only 0.5×10^6 W/m^3 during the density flat-top phase. Thus the problem originated from the power balance in the very center of this plasma: NBI central deposition was not large enough to prevent the thermal collapse as the carbon concentration and radiation increased. Although the relative concentration rise of the metallic species was even faster, their contribution to the total radiated power was small.

Another demonstration discharge was shown previously in Fig. 10 (dashed). In this discharge, a pellet was injected at $t = 2200$ ms during an otherwise ELM-free period, triggering a 15 ms L–mode phase; note the rapid $\bar{n}_e$ decay. Measurements from charge-exchange recombination spectroscopy showed a rapid reduction in carbon density from $r/a > 0.5$ (not shown in Fig. 10). Thus an interesting operational scenario may be possible — one which has naturally a low type 1 ELM frequency in which pellet injection is used to trigger type 1 ELMs and brief L–mode phases to maintain a clean plasma. Combined with sawtooth activity, this technique may prevent the impurity accumulation problem observed in these ELM-free discharges. Another solution to the impurity accumulation problem would be to increase the NBI power until type 1 ELMs are encountered, but, as discussed in Section VI, MHD activity prevented this on DIII–D.

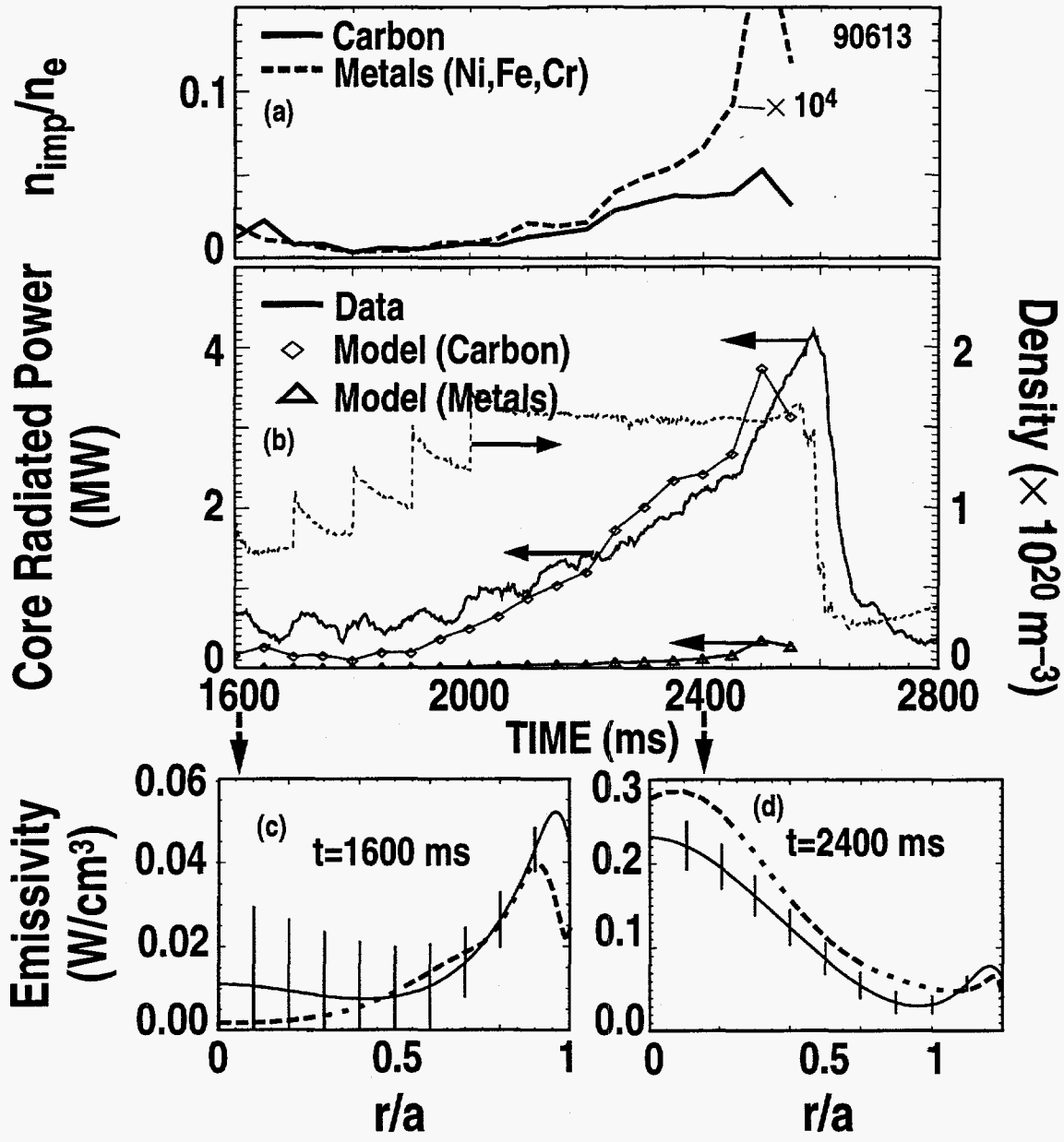

Fig. 13. MIST modeling of demonstration discharge. (a) Carbon (solid) and metals (dashed) concentration increased during density flat-top and ELM-free phase from 2000–2600 ms. Modeling used UV emission from several charge states as constraints. (b) Total radiated power from bolometry increased during density flat-top. Modeling shows most of the increase can be accounted for by carbon (diamonds). Metals (triangles) contribute only a small amount to radiated power. Measured and modeled radiated power profiles at $t = 1600$ ms (c) and 2400 ms (d) are in good agreement, in magnitude and profile shape. Data demonstrates that radiation increase originates entirely from $r/a < 0.6$ and largest emissivity increase originates from $r/a = 0$, *i.e.*, radiative collapse originates from very center of plasma.

VIII. SUMMARY AND CONCLUSIONS

By using a qualitative understanding of the processes which limit density in DIII–D, the $\bar{n}_e$ was increased up to the poloidally symmetric core radiative power balance limit, which is the most fundamental density limit in tokamaks. Demonstration discharges with $G_n \sim 1.5$ were achieved for ~ 600 ms with H–mode energy confinement, although the confinement was evolving. These discharges demonstrate the existence of an operating space with $G_n > 1$ and H–mode confinement. Thus we conclude that the path to achieving $G_n > 1$ is difficult but not impossible.

We have determined that the pellet density confinement time is independent of G_n but does increase non-linearly with I_p. In addition, we have shown that fueling profile control can be used to avoid divertor thermal collapse. Also, we have shown that MARFE formation can be avoided by low q operation, qualitatively consistent with theory. Finally, we have shown that MHD activity is observed in pellet-fueled discharges, even though calculations indicate that the plasma should be stable to these modes. Additional work is required to understand the mechanisms which drive MHD activity.

IX. ACKNOWLEDGMENTS

The first author would like to thank T.N. Carlstrom, R.J. Groebner, D.N. Hill, W.A. Houlberg, T.L. Hsieh, C.J. Lasnier, S.L. Milora, T.H. Osborne, T.H. Rhodes, B.W. Rice, R.E. Stockdale, and D.E. Thomas for stimulating discussions and diagnostic support. The Δ' calculation code was provided courtesy of Tom Gianakon from the University of Wisconsin at Madison. The efforts of the DIII–D operations staff are gratefully acknowledged.

This is a report of work sponsored by the U.S. Department of Energy under Contract Nos. DE-AC03-89ER51114, DE-AC05-96OR22464, DE-AC04-94AL8500, and W-7405-ENG-48, and Grant No. DE-FG03-86ER53266. The first author is sponsored by an Oak Ridge National Laboratory Postdoctoral Research Associate Fellowship, administered by Oak Ridge Associated Universities.

X. REFERENCES

[1]M. Greenwald, J.L. Terry, S.M. Wolfe, S. Ejima, M.G. Bell, S.M. Kaye, and G.H. Neilson, Nucl. Fusion **28**, 2199 (1988).

[2]A. Gibson, Nucl. Fusion **16**, 546 (1976).

[3]N. Ohyabu, Nucl. Fusion **19**, 1491 (1979).

[4]D.E. Roberts, Nucl. Fusion **23**, 311 (1983).

[5]F.W. Perkins and R.A. Hulse, Phys. Fluids **28**, 1837 (1985).

[6]K. Borass, Nucl. Fusion **31**, 1035 (1991).

[7]H. Niedermeyer, G. Becker, B. Bomba, H. Bruhns, K. Büchl, A. Carlson, G. Dodel, A. Eberhagen, H.-U. Fahrbach, G. Fussman, O. Gehre, K. Gentle, J. Gernhardt, L. Giannone, G.v. Gierke, E. Glock, S.v. Goeler, O. Gruber, G. Haas, H. Herrmann, J. Hoffman, E. Holzhauer, K. Hübner, G. Janeschitz, S. Kaesdorf, F. Karger, M. Kaufmann, M. Keilhacker, O. Klüber, M. Kornherr, K. Krieger, K. Lackner, R. Lang, P. Lee, G. Lisitano, M. Lörcher, T.C. Luce, F. Mast, H.M. Mayer, K. McCormick, D. Meisel, V. Mertens, Y. Miura, E.R. Müller, H. Murmann, J. Neuhauser, R. Nolte, J.M. Noterdaeme, M.P. Petrov, W. Poschenrieder, R. Preis, H. Rapp, D.E. Roberts, H. Röhr, A. Rudyj, W. Sandmann, F. Schneider, U. Schneider, G. Siller, E. Simmet, E. Speth, F. Söldner, A. Stäbler, K. Steinmetz, K.H. Steuer, U. Stroth, N. Tsois, O. Vollmer, F. Wagner, J.B. Whitley, H. Würz, and D. Zasche, Plasma Phys. and Contr. Fusion **30**, 1443 (1988).

[8]A. Stäbler, K. McCormick, V. Mertens, E.R. Müller, J. Neuhauser, H. Niedermeyer, K.-H. Steuer, H. Zohm, F. Dollinger, A. Eberhagen, G. Fussmann, O. Gehre, J. Gernhardt, T. Hartinger, J.V, Hofmann, E. Kakoulidis, M. Kaufmann, G. Kyriakakis, R.S. Lang, H.D. Murmann, W. Poschenrieder, F. Ryter, W. Sandmann, U. Schneider, G. Siller, F.X. Söldner, N. Tsois, O. Vollmer, F. Wagner, ASDEX Team, NI Group, and Pellet Injection Team, Nucl. Fusion **32**, 1557 (1992).

[9]JET Team, Plasma Phys. and Contr. Fusion **29**, 1219 (1987).

[10]P.-H. Rebut, R.J. Bickerton, and B.E. Keen, Nucl. Fusion **25**, 1011 (1985).

[11]A. Loarte, private communication, "Density Limit Experiments in JET (START and TCV)," presented at the ITER Divertor Experts Group Meeting, Naka, Japan, Oct. 1995.

[12]JT-60 Team, Plasma Physics and Controlled Fusion Research, Proc. 12th Int. Conf. Nice, 1988, Vol. 1, p. 67 (International Atomic Energy Agency, Vienna, 1989).

[13]Y. Kamada, N. Hosogane, R. Yoshino, T. Hirayama, T. Tsunematsu, Nucl. Fusion **31**, 1827 (1991).

[14]N. Asakura, Japan Atomic Energy Research Institute, private communication (March 1996).

[15]C. Weggel, W. Hamburger, B. Montgomery, N. Pierce, "Engineering Problems of Fusion Research," Vol. I, p. 54 (Oct. 1979).

[16]M.G. Bell, G.L. Schmidt, P.C. Efthimion, B. Grek, R.A. Hulse, D.K. Owens, H.K. Park, A.T. Ramsey, J.F. Schivell, and G. Taylor, Nucl. Fusion **32**, 1585 (1992).

[17]P.T. Lang, K. Buchl, J.C. Fuchs, O. Gehre, O. Gruber, R.S. Lang, M. Maraschek, V. Mertens, H. Salzmann, H. Zohm and the ASDEX-Upgrade Team, Proc. of 22nd European Conference on Controlled Fusion (European Physical Society, Petit-Lancy, Switzerland), Vol. II, p. 449 (1995).

[18]K.M. Young, M.G. Bell, W.R. Blanchard, N.L. Bretz, J. Cecchi, J. Coonrod, S. Davis, H.F. Dylla, P.C. Efthimion, R.J. Fonck, R.J. Goldston, D.J. Drove, R.J. Hawryluk, R. Little, M. McCarthy, D. McCune, K. McGuire, D. Meade, S.S. Medley, D. Mikkelsen, D. Mueller, E. Nieschmidt, D.K. Owens, A. Ramsey, A.L. Roquemore, L. Samuelson, N. Sauthoff, H. Park, J. Schivell, J.A. Schmidt, S. Sesnic, J. Sinnis, J. Strachan, G.D. Tait, G. Taylor, F. Tenny, and M. Ulrickson, Plasma Phys. Contr. Fusion 26, 11 (1984).

[19]K. Lackner, H.S. Bosch, D. Coster, O. Gruber, G. Haas, A. Herrmann, A. Kallenbach, M. Kaufmann, V. Mertens, J. Neuhauser, F. Ryter, M. Weinlich, H. Zohm, M. Albrecht, M. Alexander, K. Asmussen, M. Ballico, K. Behler, K. Behringer, M. Bessenrodt-Weberpals, M. Brambilla, K. Büchl, A. Carlson, L. Cupido, H.J. DeBlank, S. De Pena Hempel, S. Deschka, C. Dorn, R. Drube, R. Dux, A. Eberhagen, W. Engelhardt, H.-U. Fahrbach, H.-U. Feist, S. Fiedler, D. Fieg, A. Field, J.C. Fuchs, G. Fußmann, C. Garcia-Rosales, O. Genhre, J. Gernhardt, W. Herrmann, S. Hirsch, P. Ignacz, B. Jüttner, W. Junker, T. Kass, K. Kiemer, W. Köppendörfer, H.Kollotzek, M. Kornherr, K. Kreiger, B. Kurzan, P. Lang, R. Lang, M. Laux, G. Lieder, M.E. Manso, M. Maraschek, K.-F. Mast, H.-M. Mayer, P. McCarthy, D. Meisel, R. Merkel, H. Murmann, B. Napiontek, D. Naujoks, G. Neu, R. Neu, J.-M. Noterdaeme, G. Pautasso, C.S. Pitcher, W. Poschenrieder, G. Raupp, H. Richter, T. Richter, H. Röhr, J. Roth, N. Salmon, H. Salzmann, W. Sandmann, H.-B. Schilling, M. Schittenhelm, H. Schneider, R. Schneider, W. Schneider, K. Schönmann, G. Schramm, U. Schumacher, J. Schweizner, U. Seidel, F. Serra, A. Silva, M. Sokoll, E. Speth, A. Stäbler, K.-H. Steuer, J. Stober, B. Streibl, W. Suttrop, W. Treutterer, M. Troppmann, M. Ulrich, P. Varela, H. Vernickel, O. Vollmer, H. Wedler, U. Wenzel, F. Wesner, R. Wunderlich, D. Zasche. J.P. Zehrfeld, Plasma Phys. Contr. Fusion **36**, B79 (1994).

[20]T.W. Petrie, A.G. Kellman, and M.A. Mahdavi, Nucl. Fusion **33**, 929 (1993).

[21]J.L. Luxon and L.G. Davis, Fusion Technol. **8**, 441 (1985).

[22]T.W. Petrie, D.N. Hill, S.L. Allen, D. Buchenauer, J.W. Cuthbertson, Ph. Ghendrih, C.J. Lasnier, A.W. Leonard, R. Maingi, G.D. Porter, D.G. Whyte, R.J. Groebner, R. Jong, M.A. Mahdavi, S.I. Thompson, W.P. West, R.D. Wood, "Radiative Divertor Experiments in DIII–D with D_2 Injection," Nucl. Fusion in press.

[23]F.W. Perkins, D. Post, M. Rosenbluth, O. Sauter, K. Borass, D. Campbell, J.G. Cordey, M. Greenwald, T.C. Hender, Y. Kamada, R. La Haye, A. Mahdavi, A.W. Morris,

V. Mertens, J. Neuhauser, T. Taylor, H.R. Wilson, R. Yoshino, H. Zohm, "ITER Operational Limits," in Proc. of the 16th International Fusion Energy Conference, Montréal, 1996 (International Atomic Energy Agency, Vienna, Austria), in press.

[24]K. Tomabechi and the ITER Team, Nucl. Fusion **31**, 1135 (1991).

[25]The H-mode Database Working Group, Proceedings of 20th European Conference on Controlled Fusion and Plasma Physics, Europhysics Conference Abstracts, **17A**, 103 (1993).

[26]D.R. Baker, R.T. Snider, and M. Nagami, Nucl. Fusion **22**, 807 (1982).

[27]B. Lipschultz, B. LaBombard, E.S. Marmar, M.M. Pickrell, J.L. Terry, R. Waterson, and S.M. Wolfe, Nucl. Fusion **24**, 977 (1984).

[28]M.A. Mahdavi, J.C. DeBoo, C.L. Hsieh, N. Ohyabu, R.D. Stambaugh, and J.C. Wesley, Phys. Rev. Lett. **47**, 1602 (1981).

[29]L.R. Baylor, T.C. Jernigan, T.N. Carlstrom, and W.A. Houlberg, "Pellet Injection into H–mode Plasmas on DIII–D," 22nd European Conference on Controlled Fusion and Plasma Physics, Europhysics Conf. Abstracts, 19C, 133, (1995).

[30]J.P. Smith , C. Baxi, E. Reis, and L. Sevier, Fusion Technol. **21**, 1658 (1992).

[31]Ph. Ghendrih, T.W. Petrie, C. Lasnier, A.W. Leonard, and R. Maingi, J. Nucl. Mater. **220-222**, 305 (1995).

[32]D.P. Schissel, M.A. Mahdavi, J.C. DeBoo, and M. Le, Nucl. Fusion **34**, 1401 (1994).

[33]S.L. Milora, W.A. Houlberg, L.L. Lengyel, and V. Mertens, Nucl. Fusion **35**, 657 (1995); see also references therein.

[34]T.N. Carlstrom, P. Gohil, J.G. Watkins, K.H. Burrell, S. Coda, E.J. Doyle, R.J. Groebner, J. Kim, R.A. Moyer, and C.L. Rettig, Plasma Phys. Contr. Fusion **36**, A147 (1994).

[35]J. Drake, Phys. Fluids **30**, 8 (1987).

[36]J.A. Wesson and T.C. Hender, Nucl. Fusion **33**, 1019 (1993).

[37]H.P. Furth, P.H. Rutherford, and T. Selberg, Phys. Fluids **16**, 1054 (1973).

[38]C.C. Hegna and J.D. Callan, Phys. Plasmas **1**, 2308 (1994).

[39]R.J. La Haye, L.L. Lao, E.J. Strait, and T.S. Taylor, "High Beta Tokamak Operation in DIII-D Limited at Low Density/Collisionality by Resistive Tearing Modes," submitted to Nucl. Fusion.

[40]A. Weller, A.D. Cheetham, A.W. Edwards, R.D. Gill, A. Gondhalekar, R.S. Granetz, J. Snipes, and J.A. Wesson, Phys. Rev. Lett. **59**, 2303 (1987).

[41]J.A. Wesson, Plasma Phys. Contr. Fusion 37, A337 (1995).

[42]M.A. Mahdavi, D. Hill, S.L. Allen, N.H. Brooks, K.H. Burrell, T. Carlstrom, D. Content, J. DeBoo, P. Gohil, N. Gottardi, C.L. Hsieh, G. Haas, G. Jackson, N. Ohyabu, M.E. Perry, T. Petrie, M. Rensink, D. Schissel, M. Shimada, R. Snider, R. Stambaugh, R. Stockdale, and T. Taylor, J. Nucl. Mater. **162-164**, 245 (1989).

[43]The JET Team, Plasma Physics and Controlled Fusion, Proc. 12th Int. Conf. Nice, 1988, (International Atomic Energy Agency, Vienna 1989) p. 215.

[44]R.A. Hulse, Nucl. Technol./Fusion **3**, 259 (1983).